Preprints of the 21st IFAC World Congress (Virtual)
Berlin, Germany, July 12-17, 2020

Robust Tracking Control of Mechanical Hybrid Systems Driven by Electrical Actuators

Leonardo Herrera * **Yury Orlov** ** **Oscar Montaño** ***
Luis T. Aguilar **** **Ramón I. Verdés** ****

* *Department of Mechanical and Aerospace Engineering, Naval Postgraduate School, 1 University Circle, Monterey, CA 93943, USA (e-mail: leonardo.herrera@nps.edu).*
** *Department of Electrónica y Telecomunicaciones, CICESE, Carretera Tijuana-Ensenada 3918, Fracc. Zona Playitas, 22860 Ensenada, B.C., México. (e-mail: yorlov@cicese.mx)*
*** *ADSYS Controls Inc, 16 Technology Dr, Irvine, CA 92618, USA, (e-mail: montano.oscar@gmail.com)*
**** *Instituto Politécnico Nacional, CITEDI, Ave. Instituto Politécnico Nacional 1310 Colonia Nueva Tijuana, Tijuana, 22435, México, (e-mail: laguilarb@ipn.mx; rverdes@citedi.mx)*

Abstract: The primary concern of the work is the robust synthesis of hybrid electromechanical systems, operating under unilateral position constraints. The synthesis relies on the nonlinear $\mathscr{H}_\infty$ paradigm to be extended in the presence of impact phenomena, perturbations in the continuous and discrete phases, and the dynamics of the electrical actuators that drive the motion of the system. Performance issues of the proposed nonlinear $\mathscr{H}_\infty$-controller are illustrated in an experimental study of an impacting inverted pendulum.

1. INTRODUCTION

Switched dynamic systems, which are governed by coupled differential and difference equations with a switching rule between such equation, defined according to output and/or time constraints, are typically referred to as hybrid systems. These types of systems have attracted much attention due to their wide variety of applications and due to the need of special tools for their analysis. In particular, this work focuses on mechanical impact hybrid systems, otherwise known as mechanical systems subject to unilateral constraints.

As with many other types of mechanical systems, robustness proves to be a challenging issue for mechanical systems, operating under unilateral constraints. The $\mathscr{H}_\infty$ approach is well-recognized to be an effective tool of robust control of continuous-time systems, see, e.g., Isidori and Astolfi (1992), Orlov et al. (1999), and Orlov and Aguilar (2014). This technique has recently been extended in Montano et al. (2014) to the control of mechanical systems under unilateral constraints. Similar to the continuous-time frame, this technique ensures the closed-loop asymptotic stability of unperturbed mechanical systems in the presence of unilateral constraints, while also attenuating external disturbances that occur both in the continuous and discrete dynamics. The success of this technique has led to further investigations, see, e.g., Montano et al. (2016) and Montano et al. (2017). By now, such progress has been confined to mechanical systems, controlled through torque forces. However, the control inputs of mechanical systems are frequently produced through voltages applied to electrical actuators, which in turn generate the torques, enforcing the underlying electromechanical system. Being complementary to the existing literature, additional dynamics, corresponding to electrical actuators, are addressed in this paper to enhance the performance of the closed-loop electromechanical system by synthesizing voltages rather than torques to control them in the presence of unilateral position constraints.

Controlling unconstrained mechanical systems, augmented with actuator dynamics, has been addressed in the literature, e.g., in Chen et al. (1998), Wang et al. (2009), and Herrera et al. (2019). The latter work is further developed to incorporate unilateral position constraints into the present investigation. The proposed robust synthesis of mechanical systems, operating under unilateral constraints and driven by electrical actuators, constitutes the main contribution of this work. It is worth noticing that the actuator dynamics result in an inherent source of perturbations of the mechanical system under unilateral constraints, which is unavoidable in practice. Due to this, the asymptotic stability of the overall electromechanical system cannot any longer be accomplished. Meanwhile, the disturbance attenuation can be guaranteed in terms of the $\mathscr{L}_2$-gain of the closed-loop system with an appropriate attenuation level γ. Experimental results support the proposed synthesis with good performance of the closed-loop system in the presence of external disturbances that appear in both continuous and discrete phases.

The work is outlined as follows. Section 2 describes the general system under consideration. Section 3 states the control problem. Section 4 presents a case of study, including experimental results, and finally, Section 5 collects the conclusions.

2. HYBRID SYSTEM

Mechanical hybrid systems, driven by electrical actuators, to be considered in this work comply with the following generic representation of the hybrid system

$$M(\boldsymbol{q})\ddot{\boldsymbol{q}}+C(\boldsymbol{q},\dot{\boldsymbol{q}})\dot{\boldsymbol{q}}+\boldsymbol{G}(\boldsymbol{q})=B\boldsymbol{\tau}+\boldsymbol{w_q} \quad (1)$$
$$\dot{\boldsymbol{\tau}}=A_{\boldsymbol{\tau}}\boldsymbol{\tau}+B_{\boldsymbol{\tau}}\boldsymbol{\nu}+\boldsymbol{w_\tau} \quad (2)$$

evolving within a unilateral position constraint $F_0(\boldsymbol{q})>0$ and governed by a transition

$$\boldsymbol{q}(t_i^+)=\boldsymbol{q}(t_i^-) \quad (3)$$
$$\dot{\boldsymbol{q}}(t_i^+)=\theta(\boldsymbol{q}(t_i))\dot{\boldsymbol{q}}(t_i^-)+\boldsymbol{W}_i^{1d} \quad (4)$$
$$\boldsymbol{\tau}(t_i^+)=\boldsymbol{\tau}(t_i^-) \quad (5)$$

while touching the constraint $F_0(\boldsymbol{q})=0$. The continuous dynamics are governed by the well-known Euler-Lagrange equation (1) and by the electrical actuators dynamics (2) . Here, $\boldsymbol{q}(t)\in\mathbb{R}^n$ and $\dot{\boldsymbol{q}}(t)\in\mathbb{R}^n$ are the generalized position and velocity vectors, respectively; $\boldsymbol{\tau}\in\mathbb{R}^n$ describes the vector of torques associated with the actuated generalized coordinates, $\boldsymbol{\nu}(t)\in\mathbb{R}^n$ is the voltage-based control input, $M(\boldsymbol{q})\in\mathbb{R}^{n\times n}$ is the inertia matrix which is positive definite, $C(\boldsymbol{q},\dot{\boldsymbol{q}})\dot{\boldsymbol{q}}\in\mathbb{R}^n$ describes the centrifugal and Coriolis forces, $G(\boldsymbol{q})\in\mathbb{R}^n$ is for the gravitational acceleration, $B\in\mathbb{R}^{n\times n}$ describes a constant matrix that distributes the torques, $A_{\boldsymbol{\tau}}\in\mathbb{R}^{n\times n}$ and $B_{\boldsymbol{\tau}}\in\mathbb{R}^{n\times n}$ are diagonal matrices that define the behaviour of the electrical actuators, particularly $A_{\boldsymbol{\tau}}$ is a Hurwitz matrix, and the vectors $\boldsymbol{w_q}\in\mathbb{R}^n$ and $\boldsymbol{w_\tau}\in\mathbb{R}^n$ describe disturbances affecting the performance of (1)–(2). Since the vector of generalized positions $\boldsymbol{q}$ is of the same dimension as that of the control input $\boldsymbol{\nu}$, then the system in question is fully actuated.

In the transition relations (3)–(5), $\boldsymbol{q}(t_i^-)$, $\dot{\boldsymbol{q}}(t_i^-)$, and $\boldsymbol{\tau}(t_i^-)$ describe the instantaneous trajectory values before unknown collision time instants $t=t_i, i=1,2\cdots$, when the trajectory hits the surface $F_0(\boldsymbol{q}(t))=0$, whereas $\boldsymbol{q}(t_i^+),\dot{\boldsymbol{q}}(t_i^+)$, and $\boldsymbol{\tau}(t_i^+)$ describe the instantaneous trajectory values after the collisions, $\boldsymbol{W}_i^{1d}, i=1,2,\cdots$ stands for a vector of perturbations that affects the velocities during the transition, $\theta(\boldsymbol{q}(t_i))\in\mathbb{R}^{n\times n}$ is a transition matrix that depends of the generalized positions, and finally the scalar function $F_0(\boldsymbol{q})$ defines the unilateral constraint imposed on the hybrid system. Relations (3)-(5) conform a rigid surface with a simple Newton restitution law, where (4) represents the change in velocity due to the impact in position.

A reference trajectory to be tracked is given by $\boldsymbol{q}^\star$ and $\dot{\boldsymbol{q}}^\star$, and it is assumed to be periodic and subject to collisions that occur when it hits the surface $F_0(\boldsymbol{q}^\star)=0$. During the collisions this trajectory is governed by

$$\boldsymbol{q}^\star(t_i^+)=\boldsymbol{q}^\star(t_i^-) \quad (6)$$
$$\dot{\boldsymbol{q}}^\star(t_i^+)=\theta(\boldsymbol{q}^\star(t_i))\dot{\boldsymbol{q}}^\star(t_i^-),\ \ i=1,2,\ldots. \quad (7)$$

It is presumed that the reference and hybrid system trajectories hit respectively the surfaces $F_0(\boldsymbol{q}^\star)=0$ and $F_0(\boldsymbol{q})=0$ at the same time instants $t_i, i=1,2,\cdots$, i.e., $F_0(\boldsymbol{q}^\star(t_i))=0$ and $F_0(\boldsymbol{q}(t_i))=0$.

2.1 Continuous Error Dynamics

The position and velocity errors $\boldsymbol{e_p}=\boldsymbol{q}-\boldsymbol{q}^\star$ and $\boldsymbol{e_v}=\dot{\boldsymbol{q}}-\dot{\boldsymbol{q}}^\star$ are specified for the generalized coordinates $\boldsymbol{q}$(t) and $\dot{\boldsymbol{q}}(t)$ with respect to the reference position and velocities $\boldsymbol{q}^\star$ and $\dot{\boldsymbol{q}}^\star$ that can eventually be produced by, e.g., a hybrid Van der Pol oscillator presented in Orlov et al. (2016) and Herrera et al. (2017). The errors dynamics, evolving beyond the surfaces $F_0(\boldsymbol{e_p}(t_i)+\boldsymbol{q}^\star(t_i))=0$ and $F_0(\boldsymbol{q}^\star(t_i))=0$, are given by

$$\dot{\boldsymbol{e}}_{\boldsymbol{p}}=\boldsymbol{e_v} \quad (8)$$
$$\dot{\boldsymbol{e}}_{\boldsymbol{v}}=M(\boldsymbol{e_p}+\boldsymbol{q}^\star)^{-1}[-C(\boldsymbol{e_p}+\boldsymbol{q}^\star,\boldsymbol{e_v}+\dot{\boldsymbol{q}}^\star)(\boldsymbol{e_v}+\dot{\boldsymbol{q}}^\star) - \boldsymbol{G}(\boldsymbol{e_p}+\boldsymbol{q}^\star)+B\boldsymbol{\tau}+\boldsymbol{w_q}]-\ddot{\boldsymbol{q}}^\star. \quad (9)$$

Since these dynamics do not have an equilibrium in the origin when are unforced (i.e. $\boldsymbol{\tau}=\boldsymbol{w_q}=0$), the controlled torque $\boldsymbol{\tau}$ is selected in the form

$$\boldsymbol{\tau}=B^{-1}[M(\boldsymbol{q}^\star)\ddot{\boldsymbol{q}}^\star+C(\boldsymbol{q}^\star,\dot{\boldsymbol{q}}^\star)\dot{\boldsymbol{q}}^\star+\boldsymbol{G}(\boldsymbol{q}^\star)+\boldsymbol{u}], \quad (10)$$

to consequently produce the error dynamics

$$\dot{\boldsymbol{e}}_{\boldsymbol{p}}=\boldsymbol{e_v} \quad (11)$$
$$\dot{\boldsymbol{e}}_{\boldsymbol{v}}=M(\boldsymbol{e_p}+\boldsymbol{q}^\star)^{-1}[-C(\boldsymbol{e_p}+\boldsymbol{q}^\star,\boldsymbol{e_v}+\dot{\boldsymbol{q}}^\star)(\boldsymbol{e_v}+\dot{\boldsymbol{q}}^\star) - \boldsymbol{G}(\boldsymbol{e_p}+\boldsymbol{q}^\star)+M(\boldsymbol{q}^\star)\ddot{\boldsymbol{q}}^\star+C(\boldsymbol{q}^\star,\dot{\boldsymbol{q}}^\star)\dot{\boldsymbol{q}}^\star+\boldsymbol{G}(\boldsymbol{q}^\star) + \boldsymbol{u}+\boldsymbol{w_q}]-\ddot{\boldsymbol{q}}^\star, \quad (12)$$

possessing an equilibrium in the origin. It is seen that a new virtual variable $\boldsymbol{u}$ has been introduced, which, in accordance with (10), can be written as

$$\boldsymbol{u}=B[\boldsymbol{\tau}-\underbrace{(B^{-1}M(\boldsymbol{q}^\star)\ddot{\boldsymbol{q}}^\star+B^{-1}C(\boldsymbol{q}^\star,\dot{\boldsymbol{q}}^\star)\dot{\boldsymbol{q}}^\star+B^{-1}\boldsymbol{G}(\boldsymbol{q}^\star))}_{\boldsymbol{\tau}^\star}], \quad (13)$$

thereby representing the error for the variable $\boldsymbol{\tau}$, which are thus governed by the relation

$$\dot{\boldsymbol{u}}=B[\dot{\boldsymbol{\tau}}-\dot{\boldsymbol{\tau}}^\star]. \quad (14)$$

To involve the voltage input $\boldsymbol{\nu}$ into the above dynamics, the relation (2) is substituted into (14) to yield

$$\dot{\boldsymbol{u}}=B[A_{\boldsymbol{\tau}}\boldsymbol{\tau}+B_{\boldsymbol{\tau}}\boldsymbol{\nu}+\boldsymbol{w_\tau}-\dot{\boldsymbol{\tau}}^\star]. \quad (15)$$

In turn, substituting

$$\boldsymbol{\nu}=(BB_{\boldsymbol{\tau}})^{-1}[\boldsymbol{\eta}-BA_{\boldsymbol{\tau}}\boldsymbol{\tau}+B\dot{\boldsymbol{\tau}}^\star] \quad (16)$$

into (15) yields

$$\dot{\boldsymbol{u}}=\boldsymbol{\eta}+B\boldsymbol{w_\tau}. \quad (17)$$

where $\boldsymbol{\eta}(t)$ is a virtual control variable to be designed. The continuous error dynamics, evolving beyond the surfaces $F_0(\boldsymbol{e_p}(t_i)+\boldsymbol{q}^\star(t_i))=0$ and $F_0(\boldsymbol{q}^\star(t_i))=0$, defined from (1) and (2), are thus composed of the relations (11), (12), and (17).

2.2 Errors During the Transition Stage

At the collision instants t_i, $i=1,2,\ldots$, the transition errors

$$\boldsymbol{e_p}(t_i^+)=\boldsymbol{e_p}(t_i^-) \quad (18)$$
$$\boldsymbol{e_v}(t_i^+)=\theta(\boldsymbol{e_p}(t_i)+\boldsymbol{q}^\star(t_i))[\boldsymbol{e_v}(t_i^-)+\dot{\boldsymbol{q}}^\star(t_i^-)] - \theta(\boldsymbol{q}^\star(t_i))\dot{\boldsymbol{q}}^\star(t_i^-)+\boldsymbol{W}_i^{1d} \quad (19)$$

are deduced from (3) and (4). Due to (5), the torque $\boldsymbol{\tau}$ does not change its value during the collisions. Then taking into account (13), is straightforward to verify the feasibility of

$$B^{-1}\boldsymbol{u}(t_i^+)+\boldsymbol{\tau}^\star(t_i^+)=B^{-1}\boldsymbol{u}(t_i^-)+\boldsymbol{\tau}^\star(t_i^-), \quad (20)$$

which can be rewritten in terms of the transition error as

$$\boldsymbol{u}(t_i^+) = \boldsymbol{u}(t_i^-) + B\underbrace{(\boldsymbol{\tau}^\star(t_i^-) - \boldsymbol{\tau}^\star(t_i^+))}_{\boldsymbol{W}_i^{2d}}, \tag{21}$$

that corresponds to the variable $\boldsymbol{\tau}$ during this transition stage. Remarkably, (21) involves the additive term $B(\boldsymbol{\tau}^\star(t_i^-) - \boldsymbol{\tau}^\star(t_i^+))$, which acts as a perturbation for the variable $\boldsymbol{u}$ during the transition. This perturbation, which is due to the transformation (10), is inherently in force during the transition stage.

3. PROBLEM STATEMENT

The present section states the $\mathscr{H}_\infty$ control problem under unilateral constraints for the following hybrid system that possesses continuous dynamics and a transition stage.

Continuous dynamics: Evolved during $F_0(\boldsymbol{e_p},t) > 0$

$$\dot{\boldsymbol{e}} = \boldsymbol{f}(\boldsymbol{e},t) + g_1(\boldsymbol{e},t)\boldsymbol{w} + g_2(\boldsymbol{e},t)\boldsymbol{\eta} \tag{22}$$
$$\boldsymbol{z} = \boldsymbol{h_1}(\boldsymbol{e},t) + k_{12}(\boldsymbol{e},t)\boldsymbol{\eta}. \tag{23}$$

Transition stage: Happens during $F_0(\boldsymbol{e_p},t) = 0$

$$\boldsymbol{e}(t_i^+) = \boldsymbol{\mu}(\boldsymbol{e}(t_i^-),t_i) + \omega(\boldsymbol{e}(t_i^-),t_i)\boldsymbol{W}_i^d \tag{24}$$
$$\boldsymbol{z}_i^d = \boldsymbol{e}(t_i^+). \tag{25}$$

Such a problem was previously stated in Montano et al. (2014) for the error dynamics, that comply with the description (22)–(25), of mechanical hybrid systems free of dynamic actuators. As the error dynamics of the hybrid system, presented here, also comply with (22)–(25), a similar problem statement, inherited from Montano et al. (2014), is now addressed with the actuators dynamics.

Throughout, system (22)–(25) is specified with the error variable $\boldsymbol{e}^T = [\boldsymbol{e_p}\ \ \boldsymbol{e_v}\ \ \boldsymbol{u}]^T \in \mathbb{R}^{3n}$, which represents the state vector with the components, belonging to $\mathbb{R}^n$. Hereinafter, the vector $\boldsymbol{\eta} \in \mathbb{R}^n$ represents the control input; the perturbations vector during the continuous dynamics is represented by $\boldsymbol{w}^T = [\boldsymbol{w_q}\ \ \boldsymbol{w_\tau}]^T \in \mathbb{R}^{2n}$, which contains the perturbation subvector $\boldsymbol{w_q} \in \mathbb{R}^n$, associated with the Euler-Lagrange equations (1), and the perturbation subvector $\boldsymbol{w_\tau} \in \mathbb{R}^n$, associated with the dynamical actuators. The perturbation vector during the transition is described by $(\boldsymbol{W}_i^d)^T = [(\boldsymbol{W}_i^{1d})\ \ (\boldsymbol{W}_i^{2d})]^T \in \mathbb{R}^{2n}$, whereas $\boldsymbol{z} \in \mathbb{R}^{4n}$ and $\boldsymbol{z}_i^d \in \mathbb{R}^{2n}$ represent respectively the continuous output and the transition output to be controlled. The functions $\boldsymbol{f}, g_1, g_2, \boldsymbol{h_1}, k_{12}, F_0, \boldsymbol{\mu}$, and ω are of appropriate dimensions and continuously differentiable in their arguments as well as uniformly bounded in t. It is also assumed that the unforced ($\boldsymbol{w} = \boldsymbol{\eta} = 0$) error system (22)–(25) has an equilibrium into the origin, i.e., for all t, $\boldsymbol{f}(0,t) = 0, \boldsymbol{h_1}(0,t) = 0$, and $\boldsymbol{\mu}(0,0,t) = 0$.

The matrices and vectors in (22)–(25) are thus specified as

$$\boldsymbol{f}(\boldsymbol{e},t) = \begin{bmatrix} \boldsymbol{e_v} \\ M(\boldsymbol{e_p}+\boldsymbol{q}^\star)^{-1}[-C(\boldsymbol{e_p}+\boldsymbol{q}^\star,\boldsymbol{e_v}+\dot{\boldsymbol{q}}^\star)(\boldsymbol{e_v}+\dot{\boldsymbol{q}}^\star)] \\ 0_{n\times 1} \end{bmatrix} + \begin{bmatrix} 0_{n\times 1} \\ M(\boldsymbol{e_p}+\boldsymbol{q}^\star)^{-1}[-G(\boldsymbol{e_p}+\boldsymbol{q}^\star)+M(\boldsymbol{q}^\star)\ddot{\boldsymbol{q}}^\star] \\ 0_{n\times 1} \end{bmatrix} + \begin{bmatrix} 0_{n\times 1} \\ M(\boldsymbol{e_p}+\boldsymbol{q}^\star)^{-1}[C(\boldsymbol{q}^\star,\dot{\boldsymbol{q}}^\star)\dot{\boldsymbol{q}}^\star + G(\boldsymbol{q}^\star)+\boldsymbol{u}] - \ddot{\boldsymbol{q}}^\star \\ 0_{n\times 1} \end{bmatrix}, \tag{26}$$

$$g_1(\boldsymbol{e},t) = \begin{bmatrix} 0_{n\times n} & 0_{n\times n} \\ M^{-1}(\boldsymbol{e_p}+\boldsymbol{q}^\star) & 0_{n\times n} \\ 0_{n\times n} & B \end{bmatrix}, \tag{27}$$

$$g_2(\boldsymbol{e},t) = \begin{bmatrix} 0_{n\times n} \\ 0_{n\times n} \\ I_{n\times n} \end{bmatrix}, \tag{28}$$

$$\boldsymbol{h_1}^T(\boldsymbol{e},t) = [0_{1\times n}\ \ \boldsymbol{e_p}^T\rho_1\ \ \boldsymbol{e_v}^T\rho_2\ \ \boldsymbol{u}^T\rho_3], \tag{29}$$

$$k_{12}^T(\boldsymbol{e},t) = [I_{n\times n}\ \ 0_{n\times n}\ \ 0_{n\times n}\ \ 0_{n\times n}], \tag{30}$$

$$\boldsymbol{\mu}(\boldsymbol{e}(t_i^-),t_i) = \begin{bmatrix} \boldsymbol{e_p}(t_i^-) \\ \theta(\boldsymbol{e_p}(t_i)+\boldsymbol{q}^\star(t_i))[\boldsymbol{e_v}(t_i^-)+\dot{\boldsymbol{q}}^\star(t_i^-)] \\ \boldsymbol{u}(t_i^-) \end{bmatrix} + \begin{bmatrix} 0_{n\times 1} \\ -\theta(\boldsymbol{q}^\star(t_i))\dot{\boldsymbol{q}}^\star(t_i^-) \\ 0_{n\times 1} \end{bmatrix}, \tag{31}$$

and

$$\omega(\boldsymbol{e}(t_i^-),t_i) = \begin{bmatrix} 0_{n\times n} & 0_{n\times n} \\ I_{n\times n} & 0_{n\times n} \\ 0_{n\times n} & B \end{bmatrix}. \tag{32}$$

The weight matrices ρ_1, ρ_2, and ρ_3 are diagonal and of the dimension $n \times n$. The functions $\boldsymbol{h_1}$ and k_{12} are assumed to obey the well-known assumptions

$$\boldsymbol{h_1}^T(\boldsymbol{e},t)k_{12}(\boldsymbol{e},t) \equiv 0,\ \ k_{12}^T(\boldsymbol{e},t)k_{12}(\boldsymbol{e},t) \equiv I, \tag{33}$$

which are typically used in the traditional $\mathscr{H}_\infty$ synthesis design (see, e.g., Isidori and Astolfi (1992), Orlov et al. (1999), and Orlov and Aguilar (2014)), as well as in the hybrid one (see, e.g., Montano et al. (2014) and Montano et al. (2016)).

Consider a causal feedback controller

$$\boldsymbol{\eta} = \xi(\boldsymbol{e}) \tag{34}$$

with the function $\xi(\boldsymbol{e})$ of class C_1, escaping in the origin, i.e., $\xi(0) = 0$. Such a controller is said to be a *locally (globally) admissible controller* if the undisturbed ($\boldsymbol{w} = 0, \boldsymbol{W}_i^d = 0$) closed-loop system (22)–(25) is uniformly (globally) asymptotically stable.

The $\mathscr{H}_\infty$-control problem of interest consists then in finding an admissible global controller (if any) such that the $\mathscr{L}_2$-gain of the disturbed system (22)–(25) is less than a certain attenuation level $\gamma > 0$, that is the inequality

$$\int_{t_0}^{T} \|\boldsymbol{z}\|^2 \mathrm{d}t + \sum_{i=1}^{N_T} \|\boldsymbol{z}_i^d\|^2 \le \gamma^2 \left[\int_{t_0}^{T} \|\boldsymbol{w}\|^2 \mathrm{d}t + \sum_{i=1}^{N_T} \|\boldsymbol{W}_i^d\|^2 \right] + \sum_{k=0}^{N_T} \beta_k(\boldsymbol{e}(t_k^-),t_k) \tag{35}$$

is satisfied for some positive definite functions $\beta_0(\boldsymbol{e},t), \cdots, \beta_{N_T}(\boldsymbol{e},t)$ for all segments $[t_0;T]$ and a natural N_T such that $t_{N_T} \le T < t_{N_T+1}$, and for all piecewise continuous disturbances $\boldsymbol{w}$ and discrete ones $\boldsymbol{W}_i^d, i = 1,2,\cdots$.

In turn, a locally admissible controller (34) is said to be *a local solution of the $\mathscr{H}_\infty$-control problem* if there exists a neighborhood $U \in \mathbb{R}^{3n}$ of the origin, validating inequality (35) for some positive definite functions $\beta_0(\boldsymbol{e},t),\cdots,\beta_{N_T}(\boldsymbol{e},t)$, for all segments $[t_0,T]$ and a natural N_T such that $t_{N_T} \leq T < t_{N_T+1}$, for all piecewise continuous disturbances $\boldsymbol{w}$ and discrete ones $\boldsymbol{W}_i^d, i = 1,2,\cdots$ for which the state trajectory of the closed-loop system starting from an initial point $(\boldsymbol{e}(t_0) = \boldsymbol{e}_0) \in U$ remains in U for all $t \in [t_0,T]$.

3.1 Local Solution

A local solution of the problem in question is given in terms of the linearization

$$\dot{\boldsymbol{e}} \approx A(t)\boldsymbol{e} + B_1(t)\boldsymbol{w} + B_2(t)\boldsymbol{\eta} \tag{36}$$
$$\boldsymbol{z} \approx C_1(t)\boldsymbol{e} + D_{12}(t)\boldsymbol{\eta} \tag{37}$$

of the continuous dynamics (22) and (23) that evolve beyond the impact instants $t = t_i$, $i = 1,2,\ldots$ where

$$A(t) = \frac{\partial \boldsymbol{f}(\boldsymbol{e},t)}{\partial \boldsymbol{e}}|_{\boldsymbol{e}=0},\ B_1(t) = g_1(0,t),\ B_2(t) = g_2(0,t)$$
$$C_1(t) = \frac{\partial \boldsymbol{h_1}(\boldsymbol{e},t)}{\partial \boldsymbol{e}}|_{\boldsymbol{e}=0},\ D_{12}(t) = K_{12}(0,t).$$

By the time-varying strict bounded real lemma (see Orlov and Aguilar (2014)), the following condition is necessary and sufficient for the linear $\mathscr{H}_\infty$ control problem of the system (36) and (37) to has a solution. Given $\gamma > 0$,

$C1$) there exists a positive constant ε_0 such that the differential Riccati equation

$$-\dot{P}_\varepsilon = P_\varepsilon(t)A(t) + A^T(t)P_\varepsilon(t) + C_1^T(t)C_1(t)$$
$$+P_\varepsilon(t)[\frac{1}{\gamma^2}B_1B_1^T - B_2B_2^T](t)P_\varepsilon(t) + \varepsilon I, \tag{38}$$

has a uniformly bounded symmetric and positive definite solution $P_\varepsilon(t)$ for each $\varepsilon \in (0,\varepsilon_0)$.

For the nonlinear $\mathscr{H}_\infty$ control problem under unilateral constraints, this condition is also sufficient for a local solution to exist, if coupled to the next conditions:

$C2$) the norm of the matrix function ω is upper bounded by $\frac{\sqrt{2}}{2}\gamma$, i.e.,

$$\|\omega\| < \frac{\sqrt{2}}{2}\gamma; \tag{39}$$

$C3$) there exist a smooth, positive definite, decrescent function $V(\boldsymbol{e},t)$ and a positive definite function $R(\boldsymbol{e})$ such that the Hamilton-Jacobi-Isaacs inequality

$$\frac{\partial V}{\partial t} + \frac{\partial V}{\partial \boldsymbol{e}}(\boldsymbol{f}(\boldsymbol{e},t) + g_1(\boldsymbol{e},t)\alpha_1 + g_2(\boldsymbol{e},t)\alpha_2)$$
$$+\boldsymbol{h_1}^T\boldsymbol{h_1} + \alpha_2^T\alpha_2 - \gamma^2\alpha_1^T\alpha_1 \leq -R(\boldsymbol{e}) \tag{40}$$

holds with

$$\alpha_1 = \frac{1}{2\gamma^2}g_1^T(\boldsymbol{e},t)\left(\frac{\partial V}{\partial \boldsymbol{e}}\right)^T,\ \alpha_2 = \frac{1}{2}g_2^T(\boldsymbol{e},t)\left(\frac{\partial V}{\partial \boldsymbol{e}}\right)^T.$$

$C4$) condition $C3$) is satisfied with the function $V(\boldsymbol{e},t)$ that decreases along the direction $\boldsymbol{\mu}$, given by (31), in the sense that the inequality

$$V(\boldsymbol{e},t) \geq V(\boldsymbol{\mu},t) \tag{41}$$

holds in the domain of V. The following result is in force.

Theorem 1. Let condition C1 be satisfied, with some $\gamma > 0$, for the error dynamics (22)–(25) *of the mechanical hybrid system driven by actuators. Then condition C3 holds locally around the equilibrium* $(\boldsymbol{e} = 0)$ *of this dynamics with*

$$V(\boldsymbol{e},t) = \boldsymbol{e}^T P_\varepsilon \boldsymbol{e},\ \ R(\boldsymbol{e}) = \frac{\varepsilon}{2}||\boldsymbol{e}||^2 \tag{42}$$

and the closed-loop system driven by the state feedback

$$\boldsymbol{\eta} = -g_2^T(\boldsymbol{e},t)P_\varepsilon\boldsymbol{e} \tag{43}$$

locally possesses a $\mathscr{L}_2$-gain less than γ provided that the condition C2 holds as well. If additionally the condition C4 is satisfied with the quadratic function $V(\boldsymbol{e},t)$, given in (42)*, then the disturbance-free closed-loop system* (22)–(25) *and* (43) *is uniformly asymptotically stable.*

Proof of this theorem is rather technical and it follows the line of reasoning used in Montano et al. (2014). Because of space limitation, the proof is omitted to be published elsewhere. ■

Since the reference trajectory compensator, involved into the control law (10), causes a persistent perturbation that appears in the control transition (21), the above theorem, applied to the original system, is only capable of ensuring its $\mathscr{L}_2$-gain to be less than γ. The following corollary is thus straightforward.

Corollary 1. Let condition C1 be satisfied, with some $\gamma > 0$, for (22)–(25)*. Then condition C3 holds locally around the equilibrium* $(\boldsymbol{e} = 0)$ *of* (22)–(25) *with* (42) *and the closed-loop system driven by the state feedback* (43) *locally possesses a $\mathscr{L}_2$-gain less than γ provided that the condition C2 holds as well.*

Although the virtual control input $\boldsymbol{\eta}$ has been computed so far, the real voltage control input for (1)–(5) is given by (16), which comply with the control objective of the closed-loop control system (1)–(5), (16).

4. CASE OF STUDY: CONSTRAINED ACTUATOR-DRIVEN PENDULUM

A benchmark pendulum-barrier system, driven by actuator, illustrated in Fig. 1, is governed by the dynamical model (1)–(5), specified with

$$n = 1, \boldsymbol{q} = q, M(\boldsymbol{q}) = (ml^2 + J), C(\boldsymbol{q},\dot{\boldsymbol{q}})\dot{\boldsymbol{q}} = -k\dot{q}, \tag{44}$$
$$\boldsymbol{G}(\boldsymbol{q}) = mgl\sin(q), B = 1, A_\tau = -a, B_{\boldsymbol{\tau}} = 1, \boldsymbol{\tau} = \tau, \tag{45}$$
$$\boldsymbol{\nu} = \nu, \boldsymbol{W}_i^{1d} = w_i^{1d}, \theta(\boldsymbol{q}(t_i)) = -\kappa, \boldsymbol{w_\tau} = w_\tau, \boldsymbol{w_q} = w_q. \tag{46}$$

The continuous dynamics (1) and (2) operate for $q = F_0(q) \in (0,2\pi)$, whereas the transition (3)–(5) operates for $q(t_i) = F_0(q(t_i)) = 0$ when the pendulum hits the barrier. In the constrained actuator-driven pendulum, q stands for the angle between the pendulum and the barrier, nullified in its upright position, $\dot{q}$ and $\ddot{q}$ represent the first- and second-order time derivatives of q, τ describes the torque, produced by the actuator, v describes the voltage control input, m is the mass of the

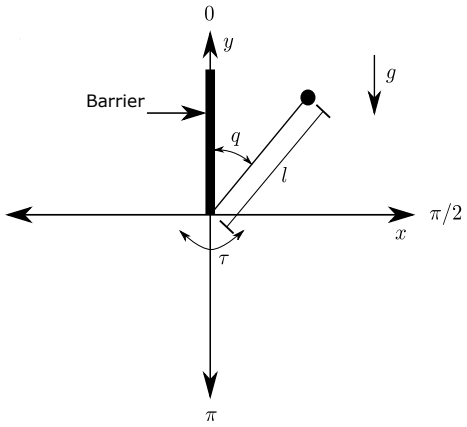

Fig. 1. Pendulum-barrier driven by actuator.

pendulum, l s ithe distance from the rotation axis to the center of mass, J is the moment of inertia of the pendulum with respect to its center of mass, g is the gravitational acceleration, k is the dry friction coefficient, a is a parameter that defines the actuator dynamics, and κ is the jump amplitude of the angular velocity, once the impact is executed.

4.1 Reference Trajectory

The reference trajectory to be tracked by the pendulum-barrier system is produced by the hybrid Van der Pol oscillator, inherited from Orlov et al. (2016) and Herrera et al. (2017). Such an oscillator is able to generate a discontinuous limit cycle, bifurcating to an asymptotically stable origin for specific parameters. Due to these features, the oscillator is attractive to be used as a reference model. Given the set $S = \{[q^\star \;\; \dot{q}^\star]^T \in \mathbb{R}^2 : q^\star = 0 \cup \dot{q}^\star \leq 0\}$, the hybrid oscillator is given by the continuous dynamic

$$\ddot{q}^\star = -\alpha \left[\left(q^{\star 2} + \frac{\dot{q}^{\star 2}}{\mu^2} \right) - \rho^2 \right] \dot{q}^\star - \mu^2 q^\star \qquad (47)$$

when $q^\star$ and $\dot{q}^\star$ don't belong to the set, and by the transition

$$\begin{aligned} q^\star(t_i^+) &= q^\star(t_i^-), \\ \dot{q}^\star(t_i^+) &= -\kappa \dot{q}^\star(t_i^-) \end{aligned} \qquad (48)$$

when $q^\star$ and $\dot{q}^\star$ are within the set. In the transition, $t_i, i = 1,2,\cdots$ are impact instants that occur when the oscillator hits the constraint. According to Herrera et al. (2017), a discontinuous limit cycle is generated by this oscillator when the bifurcation parameter values $\alpha = \mu = 1, \rho = 1.5$, and $\kappa = 0.5$ are set. Figure 2a shows this discontinuous limit cycle.

The asymptotic stability of the discontinuous limit cycle, generated under the previous stated parameter values, has been established in Herrera (2018) by applying the Poincaré map.

The error dynamics for the constrained actuator-driven pendulum with respect to the above (constrained Van der Pol) reference model system are given by relations (22)–(25) in terms of $\boldsymbol{e}^T = [\boldsymbol{e_p} \;\; \boldsymbol{e_v} \;\; \boldsymbol{u}]^T = [e_p \;\; e_v \;\; u]^T = [q - q^\star \;\; \dot{q} - \dot{q}^\star \;\; \tau - \tau^\star]^T$. Finally, the voltage-based controller for the pendulum-barrier system, driven by actuator, is given by relation (16), properly specified. With the parametric values, shown in table 1, the differential Riccati equation (38) has a positive definite and symmetric solution that satisfy the condition $C1$. The condition

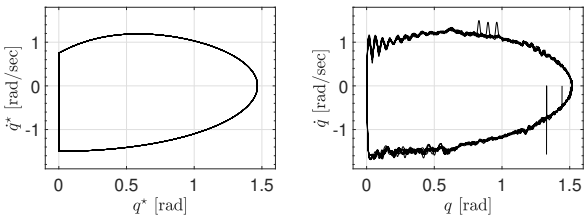

(a) Reference phase portrait $q^\star$ vs. $\dot{q}^\star$, initialized in $q^\star(0) = 0$ and $\dot{q}^\star(0) = 0.74$. Under these initial conditions and by the definition of the set S, the continuous dynamic is in force at the beginning.

(b) Phase portrait q vs. $\dot{q}$ after the transient, initialized in $q(0) = \pi$ and $\dot{q}(0) = 0$.

Fig. 2. Phase portraits

$C2$ is also satisfied with a pre-selected value of γ. According to Corollary 1, the resulting closed-loop system possesses the $\mathscr{L}_2$-gain less than γ.

4.2 Experimental Results and Discussion

Experimental results are shown in this section for the closed-loop pendulum-barrier, driven by an actuator. These results are obtained under the parametric values shown in Table 1. This table reflects the parameter values of the actuator-driven pendulum-barrier system and that of the differential Riccati equation (38).

Figure 3 shows the experimental setup consisting of a DC motor manufactured by *Leadshine* and a pendulum, hitting a vertical surface. The data are collected by the *dSPACE® 1701* prototyping hardware. The controller ran on a personal computer with a Core-i7 processor and *Matlab/Simulink®*. The amplifier of the motor accepts a control input from the D/A converter in the range of ± 10 V.

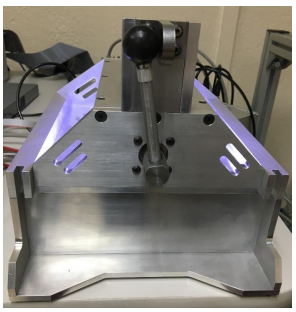

Fig. 3. The pendulum-barrier system experimental setup.

Figure 2b shows the phase portrait produced by the pendulum-barrier states; this portrait executes a small deviation with respect to the reference phase portrait of Fig. 2a. The deviation occurs after the impact, and it is due to the inherent perturbation introduced by the transformation (10), and to the peak phenomenon reported in Biemond et al. (2012).

This phenomenon is produced when the trajectory of the pendulum and the reference trajectory hit the impact surface at different times. Although the theory, developed in this paper, deals with the synchronized scenario where both trajectories hit the impact surface at the same time, for practical purposes the experiment shows either of the other two scenarios reported in Montano et al. (2016): a) the plant hits the impact surface before the reference trajectory, and b) the reference trajectory hits

Table 1.

parameter	value	unit
m	0.0474	kg
l	0.11	m
J	1×10^{-3}	kg m^2
g	9.81	m/s^2
k	0.01	N s/rad
w_q, w_τ, w_i^{1d}	0	Nm
a	5	dimensionless
κ	0.5	dimensionless
ω	1	dimensionless
γ	150	dimensionless
ρ_1	8800	dimensionless
ρ_2	1	dimensionless
ρ_3	1	dimensionless
ε	0.001	dimensionless

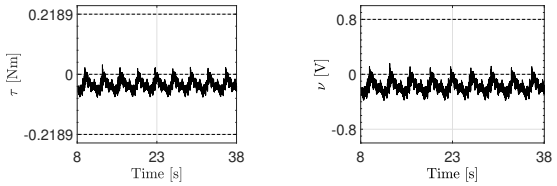

(a) Torque τ initialized in $\tau(0) = 0$. (b) Voltage v applied to the actuator.

Fig. 4. Torque and Voltage after the transient.

the impact surface before the plant trajectory. These last two cases are mainly due to the different initial conditions for the pendulum-barrier and the hybrid oscillator. As the synchronization issue during impacts is beyond the scope of this research, the peak phenomenon is involved as an additional source of error that avoids the asymptotic stability in these simulations, but eventually, it can be removed by a synchronization plant-reference method as it is shown in Montano et al. (2016).

By the attributes of the controller, the deviation respects the robustness inequality (35), thereby yielding the closed-loop system robustness. Figure 4a shows the torque produced by the actuator, whereas Fig. 4b depicts the control input, which is based on the voltage applied to the actuator, and both figures feature peaks which are due to the inherent perturbation and peak phenomenon. Because of the space limitation, the tuning procedure for the controller that would result in a suitable performance remains beyond the scope of the paper.

Since the electrical actuator dynamics are fast compared with mechanisms dynamics, they are typically admitted to be neglected in the closed-loop. However, these perform a structural perturbation that destroys the stability of the closed-loop system. In the unconstrained scenario, see Herrera et al. (2019), was shown this behavior with reasonable fast actuator dynamics. If correct, the parameters used in the unconstrained work for the actuator dynamics were extracted from a datasheet of a real electrical Pittman brand motor. Based on the unconstrained work, we hold the hypothesis that similar behavior can be presented in the constrained case. As the efforts were addressed to incorporate the dynamic of the actuator as well as to produce the first experimental results, a comparison is going to be considered in our future work.

5. CONCLUSIONS

A robust tracking controller was designed for hybrid Euler-Lagrange systems driven by electrical actuators. Although an inherent perturbation was unavoidable in the transition stage of the error dynamics as well as the peaking phenomenon was. Hence, the asymptotic tracking was not feasible; however, the robust tracking was achieved with an appropriate disturbance attenuation level. Experimental results for a benchmark pendulum-barrier system, driven by an electrical actuator, were carried out in the closed-loop to support the performance of the proposed robust synthesis.

ACKNOWLEDGMENTS

The work was supported by the Consejo Nacional de Ciencia y Tecnología under Grant 285279 and Grant A1-S-9270.

REFERENCES

Biemond, J.B., van de Wouw, N., Heemels, W.M.H., and Nijmeijer, H. (2012). Tracking control for hybrid systems with state-triggered jumps. *IEEE Transactions on Automatic Control*, 58(4), 876–890.

Chen, B.S., Uang, H.J., and Tseng, C.S. (1998). Robust tracking enhancement of robot systems including motor dynamics: A fuzzy-based dynamic game approach. *IEEE Transactions on Fuzzy Systems*, 6(4), 538–552.

Herrera, L., Montano, O., and Orlov, Y. (2017). Hopf bifurcation of hybrid Van der Pol oscillators. *Nonlinear Analysis: Hybrid Systems*, 26, 225–238.

Herrera, L., Orlov, Y., Montano, O., and Shiriaev, A. (2019). Model orbit output feedback tracking of underactuated mechanical systems with actuator dynamics. *International Journal of Control*, 0(0), 1–14.

Herrera, L.E. (2018). *Generación robusta de movimiento periódico para una clase de sistemas mecánicos subactuados con actuadores dinámicos y mediciones parciales*. Phd thesis, CICESE, Ensenada, México.

Isidori, A. and Astolfi, A. (1992). Disturbance attenuation and $\mathscr{H}_\infty$-control via measurement feedback in nonlinear systems. *IEEE Transactions on Automatic Control*, 37(9), 1283–1293.

Montano, O., Orlov, Y., and Aoustin, Y. (2014). Nonlinear state feedback $\mathscr{H}_\infty$-control of mechanical systems under unilateral constraints. *IFAC Proceedings Volumes*, 47(3), 3833–3838.

Montano, O., Orlov, Y., Aoustin, Y., and Chevallereau, C. (2017). Orbital stabilization of an underactuated bipedal gait via nonlinear $\mathscr{H}_\infty$-control using measurement feedback. *Autonomous Robots*, 41(6), 1277–1295.

Montano, O.E., Orlov, Y., and Aoustin, Y. (2016). Nonlinear $\mathscr{H}_\infty$-control under unilateral constraints. *International Journal of Control*, 89(12), 2549–2571.

Orlov, Y., Acho, L., and Solis, V. (1999). Nonlinear $\mathscr{H}_\infty$-control of time-varying systems. In *Proceedings of the 38th IEEE Conference on Decision and Control*, volume 4, 3764–3769.

Orlov, Y., Montano, O., and Herrera, L. (2016). Hopf bifurcation of Van der Pol oscillators operating under unilateral constraints. In *American Control Conference (ACC), 2016*, 5148–5153.

Orlov, Y.V. and Aguilar, L.T. (2014). *Advanced $\mathscr{H}_\infty$ control: Towards nonsmooth theory and applications*. Birkhauser, London.

Wang, L., Chai, T., and Zhai, L. (2009). Neural-network-based terminal sliding-mode control of robotic manipulators including actuator dynamics. *IEEE Transactions on Industrial Electronics*, 56(9), 3296–3304.